

# Dispersion of the temperature dependence of the retardance in SiO<sub>2</sub> and MgF<sub>2</sub>

Shelley M. Etzel, A. H. Rose, and C. M. Wang

We have directly measured the retardance versus temperature for single-crystal quartz (SiO<sub>2</sub>) and magnesium fluoride (MgF<sub>2</sub>) at wavelengths of 633, 788, 1318, and 1539 nm and over a temperature range of 24–80 °C. To our knowledge, the temperature dependence of retardance for these two materials has not been directly measured. We compared our direct measurements of the normalized temperature derivative of the retardance  $\gamma$  with derived values from previously reported indirect measurements and found our results to be in agreement and our measurement uncertainties to be typically a factor of 4 smaller. Our overall mean value for  $\gamma_{\text{SiO}_2}$  is  $-1.23 \times 10^{-4}$  with a combined standard uncertainty of  $0.02 \times 10^{-4}$  and little wavelength dependence over the 633–1539-nm range. Our overall mean value for  $\gamma_{\text{MgF}_2}$  is  $-5.37 \times 10^{-5}$  with a combined standard uncertainty of  $0.17 \times 10^{-5}$  and with a small wavelength dependence over the 633–1539-nm range. © 2000 Optical Society of America

OCIS codes: 120.5410, 120.6780, 160.4760.

## 1. Introduction

We measured the retardance versus temperature for single-crystal quartz (SiO<sub>2</sub>) and magnesium fluoride (MgF<sub>2</sub>) at wavelengths of 633, 788, 1318, and 1539 nm and a temperature range of 24–80 °C. This temperature dependence is needed for accurate prediction of wave-plate response. We also reviewed the literature and compared our results with previously reported values. Although, to our knowledge, the temperature dependence of retardance for these two materials has not been directly measured before, we were able to use the earlier measurements of the changes in crystal axis refractive index with temperature to estimate the temperature dependence of the retardance for SiO<sub>2</sub> and MgF<sub>2</sub>.

## 2. Background

SiO<sub>2</sub> and MgF<sub>2</sub> are birefringent optical materials used to make wave plates, polarizers, windows, and lenses. Our specific interest in these materials is their use as wave plates. Wave plates transform the

polarization state of light passing through them because of the birefringence of the crystal. Birefringence is the difference in the refractive indices between the extraordinary ( $n_e$ ) and the ordinary ( $n_o$ ) crystal axes. The orthogonal components of a polarized beam along the two crystal axes travel at different speeds. The accumulated phase shift between the two components at the output of the wave plate changes the beam's polarization state. Retardance is a measure of the accumulated phase shift as the beam passes through the wave plate and can be expressed as

$$\delta = \frac{2\pi}{\lambda} Bh, \quad (1)$$

where  $\delta$  is the retardance,  $\lambda$  is the wavelength,  $B$  is the birefringence ( $n_e - n_o$ ), and  $h$  is the thickness of the wave plate. When  $\delta > 2\pi$ , the retarder is of multiple order. Then retardance can be written as  $\delta = \delta_0 + 2\pi m$  where the order  $m$  is an integer greater than 0 and  $\delta_0$  is less than  $2\pi$  (a full wave of retardance).

Retardance  $\delta$  is dependent on temperature, because the birefringence  $B$  and the thickness  $h$  of the wave plate change with temperature. To predict wave-plate response accurately over a wide temperature range, the temperature dependence of the re-

---

The authors are with the National Institute of Standards and Technology, U.S. Department of Commerce, 325 Broadway, Boulder, Colorado 80303-3328. S. M. Etzel's e-mail address is etzel@boulder.nist.gov.

Received 17 April 2000; revised manuscript received 11 July 2000.

0003-6935/00/315796-05\$15.00/0

© 2000 Optical Society of America

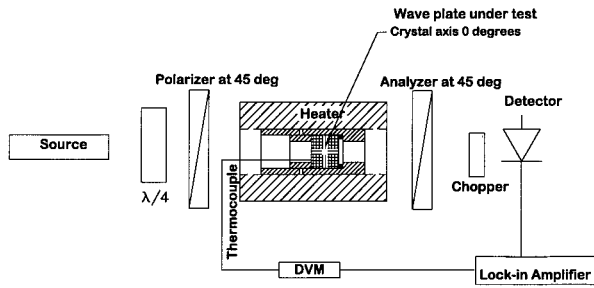


Fig. 1. Automated polarimeter arrangement for the measurement of the temperature dependence of the retardance. DVM, digital voltmeter.

retardance must be known. The temperature dependence of the retardance is

$$\frac{d\delta}{dT} = \frac{2\pi}{\lambda} \left( B \frac{dh}{dT} + h \frac{dB}{dT} \right), \quad (2)$$

where  $T$  is the temperature.

Normalizing Eq. (2), we can produce the following expression:

$$\gamma = \frac{1}{\delta} \frac{d\delta}{dT} = \frac{1}{B} \frac{dB}{dT} + \frac{1}{h} \frac{dh}{dT}, \quad (3)$$

where  $\gamma$  is the normalized temperature derivative of the retardance.

This can also be written as

$$\gamma = \frac{1}{B} \left( \frac{dn_e}{dT} - \frac{dn_o}{dT} \right) + \alpha, \quad (4)$$

where  $\alpha$  is the thermal expansion ( $1/h \, dh/dT$ ) and the temperature dependence of the birefringence is  $dB/dT = dn_e/dT - dn_o/dT$ . Earlier researchers measured these values,<sup>1–3</sup> and we used their results with Eq. (4) to estimate  $\gamma$  for our comparisons.

The temperature dependences of the refractive indices ( $dn_e/dT$  and  $dn_o/dT$ ) of  $\text{SiO}_2$  have been measured over a wavelength range of 450–1600 nm at temperatures from room temperature to 400 °C.<sup>1</sup> The thermal expansion  $\alpha$  for  $\text{SiO}_2$  is  $13.37 \times 10^{-6}/\text{°C}$  over a temperature range of  $-0.15$ – $80$  °C.<sup>2</sup> Previous researchers measured  $dn_e/dT$  and  $dn_o/dT$  for  $\text{MgF}_2$  by an interferometric technique at laser wavelengths of 457.9, 632.8, and 1150 nm at 20° temperature steps from  $-180$  to 200 °C.<sup>3</sup> The same apparatus and technique were used to measure thermal expansion  $\alpha$  for  $\text{MgF}_2$  ( $9.05 \times 10^{-6}/\text{°C} \pm 0.96 \times 10^{-6}$ ).<sup>3</sup>

In this paper we describe our direct measurement of  $\gamma$  for  $\text{SiO}_2$  and  $\text{MgF}_2$ . We then compare our results with those derived using Eq. (4) and the results from Refs. 1–3.

### 3. Procedure

#### A. Polarimetric System

We used an automated polarimeter (Fig. 1) designed for our standard retarder measurements<sup>4</sup> to measure

$\gamma$ . The automated polarimeter locates the axes of the wave plate and arranges the polarizer and analyzer axes to 45° relative to the wave-plate axes. This alignment procedure allows a linearly polarized beam to bisect the axes of the wave plate so that equal power is on each axis,  $n_e$  and  $n_o$ . The light intensity passed by the analyzer depends on the polarization state exiting the wave plate. As the retardance of the wave plate changes with temperature, the output polarization state changes. The change in retardance can be calculated from the change in transmission through the analyzer.

The theoretical response function of a wave plate placed between an aligned polarizer and analyzer in such a system is given by

$$R(T) = A \cos^2 \left[ \frac{\delta(T)}{2} \right], \quad (5)$$

or

$$R(T) = A \sin^2 \left[ \frac{\delta(T)}{2} \right], \quad (6)$$

where  $R(T)$  is the optical power at the detector and  $A$  is the optical power in the system. The  $\sin^2$  function is obtained when the polarizer and analyzer are crossed, and the  $\cos^2$  function is obtained when the polarizer and analyzer are parallel to each other. To achieve this response, care must be taken in the selection and orientation of sources, polarizers, detectors, and quarter-wave plates.

#### B. Sources

The selection and characterization of the source are important, because retardance depends on wavelength [Eq. (1)]. A broadband source adds uncertainty and noise to the measured value, because each wavelength from the source experiences a different retardance, and the output state becomes a combination of all the accumulated phase shifts. We selected laser diode sources at wavelengths of approximately 788, 1318, and 1539 nm. We measured the spectrum of each diode source with an optical spectrum analyzer. We used a weighted mean average to calculate the mean wavelength for each multiline source. We calculated the center wavelength for each Gaussian source from its FWHM. The wavelength uncertainty is shown with our results in Tables 1 and 2. We also used a He–Ne gas laser at 632.8 nm.

#### C. Detectors

We used a 5-mm-diameter germanium photodiode detector for the 633- and 788-nm measurements and a 3-mm-diameter InGaAs detector for the 1318- and 1539-nm measurements. The photodiodes were in a transimpedance amplifier configuration, and the output of the amplifier was sent to a lock-in amplifier.

Table 1. MgF<sub>2</sub>

$\lambda$ (nm) $\pm 2\sigma$	$-\gamma \times 10^5$	$2\sigma \times 10^5$	Standard Error <sup>a</sup>	Number of Measurements	Research Group
457.9	3.81	1.70			Feldman <i>et al.</i> <sup>3</sup>
633	3.60	1.62			Feldman <i>et al.</i> <sup>3</sup>
	3.8				Hale and Day <sup>5</sup>
632.8 <0.1	5.55	0.23	0.003	14	NIST <sup>b</sup>
788.73 $\pm 2.4$	5.03	0.44	0.04	36	NIST
850	3.9				Hale and Day <sup>5</sup>
1150	3.97	6.94			Feldman <i>et al.</i> <sup>3</sup>
1300	4.1				Hale and Day <sup>5</sup>
1318.2 $\pm 0.9$	5.95	0.30	0.03	23	NIST
1538.89 $\pm 1.78$	5.05	0.06	0.009	11	NIST

<sup>a</sup>Standard error,  $1\sigma/\sqrt{n}$ .

<sup>b</sup>NIST, National Institute of Standards and Technology.

#### D. Quarter-Wave Plates

We selected zero-order quarter-wave plates for each source wavelength to provide a circular polarization state at the input to the first polarizer. The automated polarimeter requires that the polarizer and analyzer rotate in an iterative fashion to locate the axes of the test wave plate. A linear state incident on the first polarizer could result in a false null, i.e., a false selection of the wave-plate axes.

#### E. Polarizers

The polarizer and analyzer are Glan–Thompson calcite prism polarizers. They provide an extinction ratio of greater than  $-55$  dB over a wavelength range of 320–2300 nm.

#### F. Specimen Preparation

Specimens of both SiO<sub>2</sub> and MgF<sub>2</sub> were cut and polished to form multiorder wave plates with their optic axes parallel to the face and perpendicular to the direction of propagation. The quartz wave plate has a diameter of  $14.55 \pm 0.13$  mm and a thickness of  $6.99 \pm 0.13$  mm. The MgF<sub>2</sub> wave plate has a diameter of  $15.70 \pm 0.13$  mm and a thickness of  $25.60 \pm$

0.13 mm. To minimize internal reflections, both wave plates were antireflection coated to provide  $<0.1\%$  reflection for the wavelength region of approximately 1250–1700 nm. We visually inspected each wave plate for stress birefringence by viewing its entire aperture with a white-light source and the wave plate between crossed polarizers. We rejected a sample that displayed light and dark bands across its face.

The test wave plate was held in an aluminum cylinder. Care was taken to not stress the wave plate. A retaining ring (locked with set screws) and a silicone O ring were used to hold the wave plate in place, and minimal pressure was applied. The wave-plate cylinder was slipped into a cylindrical heater, and the heater was held rigidly. This stable mechanical mounting was necessary to minimize changes in thickness or path length because of motion of the wave plate.

After we established the axes, the temperature of the wave plate at the entrance face and the intensity of light at the photodetector were recorded. A lock-in amplifier was used with a mechanical chopper to record the optical intensity. During the 2-h heat-

Table 2. SiO<sub>2</sub>

$\lambda$ (nm) $\pm 2\sigma$	$-\gamma \times 10^5$	$2\sigma \times 10^5$	Standard Error <sup>a</sup>	Number of Measurements	Research Group
609.5 $\pm 9.2$	1.45	0.13			Toyoda and Yabe <sup>1</sup>
632.8 <0.1	1.213	0.024	0.004	9	NIST <sup>b</sup>
633	1.3				Hale and Day <sup>5</sup>
643	1.01				Micheli <sup>2,7</sup>
787.63 $\pm 1.7$	1.196	0.028	0.008	7	NIST
850	1.4				Hale and Day <sup>5</sup>
850.5 $\pm 7.0$	1.32	0.11			Toyoda and Yabe <sup>1</sup>
1211 $\pm 17$	1.10	0.09			Toyoda and Yabe <sup>1</sup>
1300	1.7				Hale and Day <sup>5</sup>
1318.2 $\pm 0.9$	1.25	0.04	0.005	14	NIST
1408.5 $\pm 7.0$	2.05	0.45			Toyoda and Yabe <sup>1</sup>
1525 $\pm 45^c$	0.9	0.4		9	Williams <sup>9</sup>
1538.89 $\pm 1.78$	1.25	0.04	0.007	9	NIST

<sup>a</sup>Standard error,  $1\sigma/\sqrt{n}$ .

<sup>b</sup>NIST, National Institute of Standards and Technology.

<sup>c</sup>Range.

ing cycle, the temperature was linearly raised from room temperature ( $\sim 24^\circ\text{C}$ ) to nearly  $80^\circ\text{C}$ . Approximately 200 data points were taken during the heating and cooling cycle. (Some data were taken only during the heating cycle.)

#### 4. Analysis

In our arrangement we selected a wave plate of sufficient thickness and a large enough temperature range so that the response function  $R(T)$  passed through a maximum, allowing for a measure of  $A$ , the system transmission. Ideally, the polarizers would be perfect, and the source would be a single wavelength. However, the polarizers do have some leakage, and the source has a finite bandwidth. This allows some light to pass through the system that is not affected by temperature, and the system temperature response is flattened, because each wavelength component of the source experiences a slightly different retardance. The system output is a sum of the individual response functions. Thus  $A$  is the sum of  $A_0$  (representing the leakage of the polarimetric arrangement and source bandwidth effects) and  $A_1$  (representing the amplitude of the wave-plate modulation). The following equation describes the system temperature response as

$$R(T) = A_0 + A_1 \cos^2 \left\{ \frac{\pi h_0 B_0}{\gamma} [1 + \gamma(T - T_0)] \right\}, \quad (7)$$

where  $A_0$  is the amplitude difference between the minimum value and zero transmittance,  $A_1$  is the maximum amplitude minus  $A_0$ ,  $h_0$  is the thickness of the wave plate, and  $B_0$  is the birefringence at room temperature  $T_0$ . The fitting routine provides a small correction (typically 0.1–1.0%) to  $h_0$ ,  $B_0$ , and  $\lambda$ , because these values have some uncertainty. Equation (7) assumes a source with a single wavelength (zero bandwidth) and corrects for bandwidth effects in an *ad hoc* fashion through  $A_1$  and  $A_0$ .

We checked the effect of the source bandwidth on the estimate of  $\gamma$  by performing a least-squares fit to data with the following equation:

$$R(T) = A \int \cos^2 \left\{ \frac{\pi h_0 B_0}{\lambda} [1 + \gamma(T - T_0)] \right\} S_w(\lambda) d\lambda, \quad (8)$$

where  $S_w(\lambda)$  is the source bandwidth weighting function. The weighting function is normalized so that  $\int S_w(\lambda) d\lambda = 1$ . We found that the difference between the estimates of  $\gamma$  using both Eqs. (7) and (8) was not significant for laser diodes with a Gaussian wavelength distribution. The fits for the multiline diode sources showed no significant change in  $\gamma$  for the  $\text{SiO}_2$  wave plate and a small change for the  $\text{MgF}_2$  wave plate. The  $\text{MgF}_2$  wave plate is of a higher order than the  $\text{SiO}_2$  plate ( $m \approx 475$  versus  $m \approx 100$ ), and we suspect that the change we see using the multiline fit [Eq. (8)] is due to the  $\text{MgF}_2$  wave plate's greater wavelength dependence.

To derive  $\gamma$  from our experimental data, it is nec-

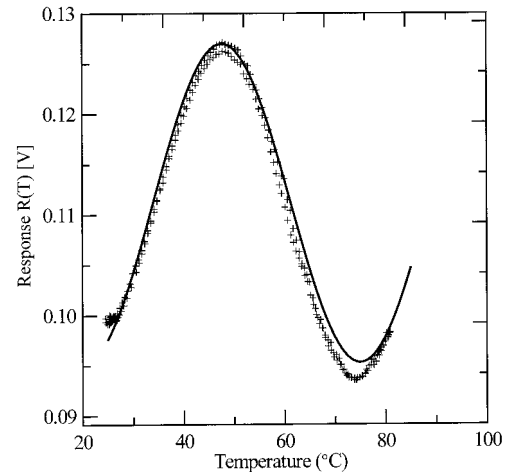


Fig. 2.  $\text{MgF}_2$  wave-plate response  $R(T)$  during heating and cooling cycle at  $789.83\text{ nm}$ : +, data values; solid curve, least-squares fit to Eq. (7).

essary to have a confident value of  $A_1$  [Eq. (7)]. Figure 2 displays the recorded response of the  $\text{MgF}_2$  wave plate as the temperature varied during the heating and cooling cycle at  $\lambda \approx 790\text{ nm}$ . The solid curve is the least-squares fit of the data to the model [Eq. (7)] with  $A_0$ ,  $A_1$ ,  $\gamma$  and the small correction to  $h_0$ ,  $B_0$ , and  $\lambda$  as fitting parameters.

To determine  $\gamma$ , a data set from an experimental run was fit to Eqs. (7) or (8). If the standard deviation of residuals from the least-squares fit was less than  $5 \times 10^{-3}$ , we used the calculated  $\gamma$ . We used the collection of  $\gamma$  values from individual runs to calculate a mean and a standard deviation. The number of runs used is shown in Table 1 ( $\text{MgF}_2$ ) and Table 2 ( $\text{SiO}_2$ ).

## 5. Results

### A. $\text{MgF}_2$

In general we measured a higher value of  $\gamma$  for  $\text{MgF}_2$  than had been previously reported. Table 1 and Fig. 3 display our fitted experimental results for  $\text{MgF}_2$  along with derived and reported values from earlier research.<sup>3,5</sup> Our wavelength and  $\gamma$  error bars at  $788.73\text{ nm}$  in Table 1 were determined from an average of measurements made with two different diode lasers.

We used Eq. (4) with previously published values of  $\alpha$ ,  $B$ ,<sup>6</sup> and temperature derivatives ( $dn_e/dT$ ,  $dn_o/dT$ ) of the crystal refractive indices to derive an estimate of  $\gamma$  for our comparisons. Feldman *et al.*<sup>3</sup> measured and tabulated  $dn_e/dT$  and  $dn_o/dT$  at 20, 40, 60, and  $80^\circ\text{C}$ . They measured and tabulated  $a$  at the same temperatures. We took these values and calculated  $\gamma$  at each temperature and used the mean of the four values of  $\gamma$  for the value in Table 1. Feldman *et al.* gave a standard deviation for the  $dn_e/dT$  and  $dn_o/dT$  measurements but not for thermal expansion  $a$ . However, they reported that their measured values for  $a$  were in close agreement with previously published research. Their sources were laser wave-

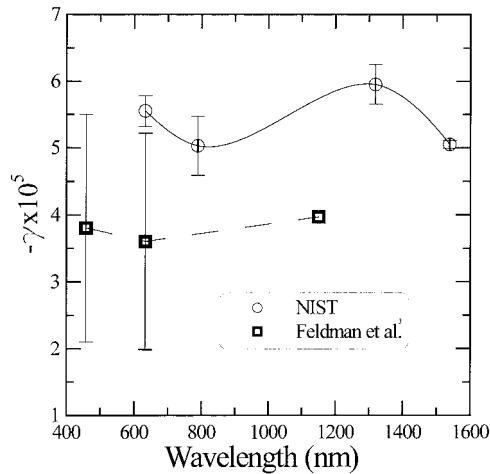


Fig. 3. Temperature dependence of the retardance for  $\text{MgF}_2$  from the National Institute of Standards and Technology (NIST) and Feldman *et al.*<sup>3</sup> Error bars are  $2\sigma$ . Curves represent spline fits.

lengths, and the wavelength uncertainty was not given. Error bars for the measurements by Feldman *et al.* at 1150 nm are not shown in Fig. 3 because they are too large for the graph. Values of Hale and Day<sup>5</sup> are an estimate from the work of Feldman *et al.*

#### B. $\text{SiO}_2$

We found that  $\gamma$  for  $\text{SiO}_2$  was slightly lower than previously measured (Table 2), but more notably it differed from past results, which had shown an increase in  $\gamma$  with wavelength for the longest wavelengths measured (Fig. 4). From the research of Toyoda and Yabe<sup>1</sup> no real trend with wavelength can be determined, and the variations may be due to experimental uncertainties.

We calculated  $\gamma$  from Toyoda and Yabe (Table 2) by

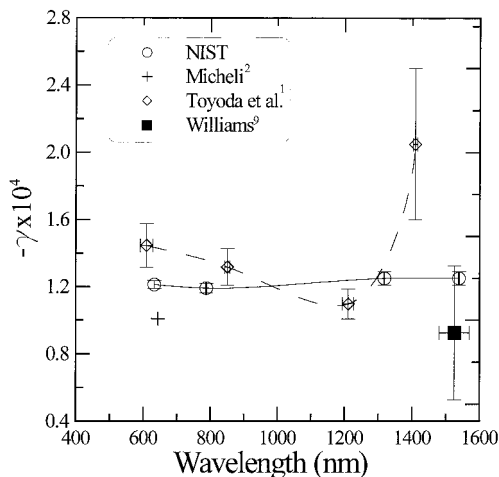


Fig. 4. Temperature dependence of the retardance for  $\text{SiO}_2$  from the National Institute of Standards and Technology (NIST) and others.<sup>2,7</sup> Error bars are  $2\sigma$ . Curves represent spline fits.

using their measured  $dn_e/dT$  and  $dn_o/dT$  and  $\alpha$  and  $B$  from Ref. 2. Results of Toyoda and Yabe were given on a graph, and we estimated the values of the measurements and the wavelengths from the graph. They showed  $dn_e/dT$  and  $dn_o/dT$  and error bars, which we assumed to be  $2\sigma$ . The wavelength error bars for Toyoda and Yabe (Fig. 4) come from our reading of the two graphs. Values by Hale and Day<sup>5</sup> are an estimate from the work of Toyoda and Yabe. Micheli measured  $dn_e/dT$  and  $dn_o/dT$  in a quartz prism and tabulated his results (without showing uncertainties).<sup>2,7</sup> Williams's value of  $\gamma$  was derived from measurements of the temperature-dependent wavelength shift of the differential group-delay curve for a polarization-mode-coupled quartz artifact.<sup>8,9</sup>

#### 6. Conclusions

We have made, to our knowledge, the first direct measurement of  $\gamma$  (normalized temperature dependence of retardance) for  $\text{SiO}_2$  ( $\text{SiO}_2$ ) and magnesium fluoride ( $\text{MgF}_2$ ). We show the mean value of  $\gamma$  for each wavelength measured and the standard deviation for each set of measurements of  $\gamma$ . We have compared our direct measurements of  $\gamma$  with derived values from previously reported indirect measurements and find our measurement uncertainties to be typically a factor of 4 smaller. Our overall mean value for  $\gamma_{\text{SiO}_2}$  is  $-1.23 \times 10^{-4}$  with a combined standard uncertainty of  $0.02 \times 10^{-4}$ , with little wavelength dependence over the 633–1539-nm range. Our overall mean value for  $\gamma_{\text{MgF}_2}$  is  $-5.37 \times 10^{-5}$  with a combined standard uncertainty of  $0.17 \times 10^{-5}$ , with a small wavelength dependence over the 633–1539-nm range.

#### References

1. T. Toyoda and M. Yabe, "The temperature dependence of the refractive indices of fused silica and crystal quartz," *J. Phys. D* **16**, L97–L100 (1983).
2. W. L. Wolfe, "Properties of optical materials," in *Handbook of Optics*, W. G. Driscoll and W. Vaughan, eds. (McGraw-Hill, New York, 1978), Chap. 7, pp. 7-82–7-134.
3. A. Feldman, D. Horowitz, R. M. Waxler, and M. J. Dodge, "Optical materials characterization," Natl. Bur. Stand. (U.S.) Tech. Note 993 (U.S. GPO, Washington D.C., 1979).
4. P. A. Williams, A. H. Rose, and C. M. Wang, "Rotating-polarizer polarimeter for accurate retardance measurement," *Appl. Opt.* **36**, 6466–6472 (1997).
5. P. D. Hale and G. W. Day, "Stability of birefringent linear retarders (waveplates)," *Appl. Opt.* **27**, 5146–5153 (1988).
6. M. J. Dodge, "Refractive properties of magnesium fluoride," *Appl. Opt.* **23**, 1980–1985 (1984).
7. F. J. Micheli, "Ueber den einfluss der temperatur auf die dispersion ultravioletter strahlen in flusspat, steinsalz, quarz und kalkspat," *Ann. Phys. (Leipzig)* **31**, 772–789 (1902).
8. P. A. Williams, "Mode-coupled artifact standard for polarization-mode dispersion: design, assembly, and implementation," *Appl. Opt.* **38**, 6498–6507 (1999).
9. P. A. Williams, Optoelectronics Division, National Institute of Standards and Technology, 325 Broadway, Boulder, Colo. 80305 (personal communication, 2000).